Search for anomalously heavy nuclei in gold and iron

D. Javorsek II,[1,*] D. Elmore,[1] E. Fischbach,[1,†] D. Granger,[2] T. Miller,[1] D. Oliver,[3] and V. Teplitz[4,‡]
[1]*Department of Physics, Purdue University, West Lafayette, Indiana 47907*
[2]*Department of Earth and Atmospheric Sciences, Purdue University, West Lafayette, Indiana 47907*
[3]*Department of Geological Sciences, Southern Methodist University, Dallas, Texas 75275*
[4]*Department of Physics, Southern Methodist University, Dallas, Texas 75275*
(Received 4 November 2001; published 1 April 2002)

There are a number of theoretical motivations for searching for anomalously heavy isotopes ${}_{Z}X$ of known elements, where Z is the nuclear charge of the anomalous nucleus X. Such nuclei could arise from the binding of a new strongly interacting massive particle (SIMP) to the nucleus of a known element, and could thus be detected as an anomalously heavy isotope of that element. SIMPs have been proposed as candidates for dark matter, and for the lightest supersymmetric particle, as well as a possible explanation for ultra high-energy cosmic rays. A search for anomalous nuclei X has been performed by analyzing several unique samples including gold nuggets collected in Australia, Arizona and North Carolina, gold foils flown on NASA's LDEF satellite, and an Fe meteorite. In each gold sample we scanned for Au isotopes with masses up to 1.67 TeV/c^2 using PRIME Lab, the Purdue accelerator mass spectrometer facility. We have also searched for anomalous Fe isotopes with masses up to 0.65 TeV/c^2 in the iron meteorite sample. We find no evidence for SIMPs in any of our samples, and our results set stringent limits on the abundance of anomalous isotopes of ordinary matter as a function of X mass.

DOI: 10.1103/PhysRevD.65.072003 PACS number(s): 14.80.−j, 26.35.+c, 82.80.Ms, 95.35.+d

I. INTRODUCTION

The object of the present paper is to describe in detail an experiment that we have recently carried out [1,2] searching for anomalously heavy Au and Fe nuclei. This search was primarily motivated by theoretical suggestions that new strongly interacting massive particles (SIMPs) exist in nature which bind to the nuclei of ordinary atoms. SIMPs could thus be detected in a search for anomalously heavy isotopes of ordinary nuclei, specifically Au and Fe in the present experiment. Although similar searches have been carried out previously for SIMPs bound to light nuclei [3], for charged SIMPs in Fe [4], and in scattering experiments [5,6], this is the first search for SIMPs bound to heavy nuclei.

The choice of gold, which is the primary focus of the present paper, was dictated by a number of considerations: (1) From an experimental point of view, gold readily forms negative ions, which the accelerator mass spectrometer (AMS) at the Purdue Rare Isotope Measurement Laboratory (PRIME Lab) requires in the sample injection stage (see Fig. 1). (2) Gold samples with reasonably well-known long exposure times to cosmic rays and/or to a component of dark matter are easier to find than would be the case for other elements, since gold is relatively unreactive (see discussion in Sec. III below). (3) There is an additional theoretical reason for searching in gold: Since a heavy nucleus is larger than a light nucleus and hence has a larger potential well, it follows from the uncertainty principle that a particle trapped in a heavier nucleus would have a smaller momentum and thus a smaller kinetic energy. As a result, SIMPs may bind preferentially to heavy nuclei [1,2,7–9]. We have also carried out a search for SIMPs in a sample obtained from an iron meteorite which we describe in greater detail below.

There are a number of theoretical motivations for searching for anomalously heavy isotopes of known elements. Among these is the suggestion that SIMPs may exist and bind to nuclei of known elements. SIMPs could thus be detected as anomalously heavy isotopes of the corresponding elements. The theoretical motivation for SIMPs arises from a number of sources. SIMPs have been suggested as candidates for dark matter [9–13], as explanations for cosmic rays with energies exceeding the Greisen-Zatsepin-Kuzmin cutoff [14–17], and as candidates for the lightest supersymmetric particle [17–23]. In addition Spergel and Steinhardt have recently proposed a model of dark matter which assumes that SIMPs exist and interact strongly with one another [24,25]. For a more detailed discussion of these theoretical motivations for SIMPs see Refs. [7] and [26].

The outline of the present paper is as follows: In Sec. II we discuss the experimental method in detail, and in Sec. III we describe the various gold and iron samples analyzed in this experiment. Section IV presents our results and our conclusions are contained in Sec. V.

II. PRINCIPLE OF THE EXPERIMENT

We present in this section a detailed description of the experimental method for detecting anomalously heavy ${}_{79}$Au and ${}_{26}$Fe nuclei using the AMS facility at PRIME Lab (see Fig. 1). The gold and iron samples were introduced into the ion source where an Au^- or Fe^- beam was formed by a 6 keV Cs^+ beam sputtering the exposed surface. The Au or Fe ions produced in the source were separated from possible

*Present address: 80th Flying Training Wing, Sheppard AFB, TX 76311.
†Corresponding author.
‡Present address: Office of Science and Technology Policy, Executive Office of the President, Washington, DC 20502.

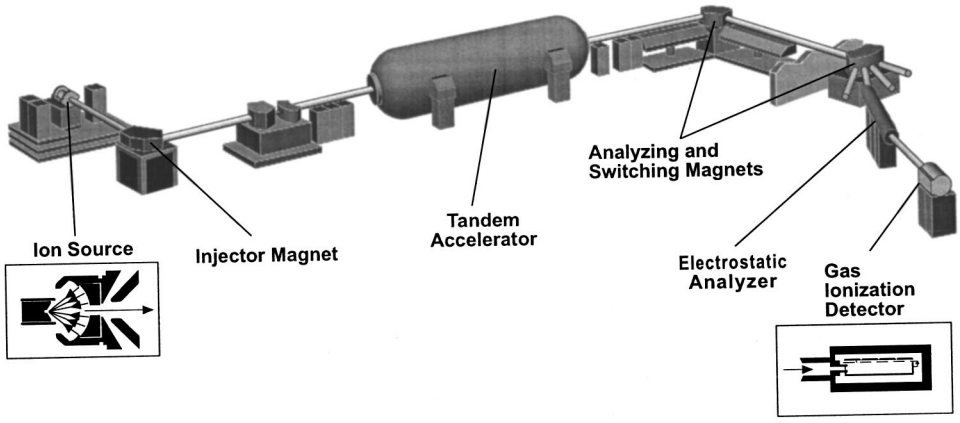

FIG. 1. Sketch of the PRIME Lab accelerator mass spectrometer.

contaminants by a 90° injector magnet, and were then accelerated to the terminal. At the terminal the ions were passed through a region containing argon gas which had the effect of removing several electrons. One purpose of this ''stripping'' stage is to dissociate any molecular contaminants present in the beam. The dissociation of molecules into individual atoms occurs for molecules with a final charge state greater than $+3$, and is often referred to as the ''Coulomb explosion.'' This arises from the circumstance that partially shielded nuclei repel one another owing to their net positive charge. As a result, contamination from a heavy molecule which could simulate the presence of an anomalously heavy isotope is significantly reduced. Another consequence of stripping is that the sign the ion charge changes, thus allowing the tandem to accelerate atoms both into and out of the accelerator.

A. Guide beams

The $_{79}$Au and $_{26}$Fe ions emerging from the accelerator are focused by the electrostatic quadrupole before entering the magnetic elements located at the high energy end. These magnetic components select for ions with a predetermined value of ME/q^2, so that for any two ions

$$\frac{M_1E_1}{q_1^2}=\frac{M_2E_2}{q_2^2}, \tag{1}$$

where M is the ion mass, E is its the energy, and q is the final charge state which results from the stripping process mentioned above. Before entering the detector, additional selection is provided by the electrostatic analyzer which selects for a predetermined value of E/q,

$$\frac{E_1}{q_1}=\frac{E_2}{q_2}. \tag{2}$$

Substituting Eq. (2) into (1) leads to

$$\frac{M_1}{q_1}=\frac{M_2}{q_2}, \tag{3}$$

and hence the net effect of these magnetic and electrostatic components is to bend the ion beam in such a way that ions with a predetermined M/q reach the gas ionization detector.

As can be seen from the preceding discussion, it is possible for species which do not have the proper mass to pass through the AMS and simulate an anomalously heavy isotope. Any beam with these characteristics is referred to as a guide beam. We are able to capitalize on this observation to create guide beams which are used to test the tune in uncharted regions of the AMS operational phase space. A guide beam is an elemental beam of conventional atoms whose M/q we may anticipate knowing *a priori* which nuclei are present in the sample. For example, gold ($M=197$ amu) in charge state $q=+5$ is a guide beam to test the tune of the AMS at $M_X=276$ amu running at charge state $q=+7$. (For a more in-depth discussion regarding guide beams see Ref. [7].) We note in passing that in addition to guide beams containing the actual samples Au and Fe, we also utilized Cu guide beams which originated from the copper cathode that housed the samples.

B. Beam detection and detector window

The gas ionization detector at PRIME Lab uses low pressure propane gas and a low transverse electric field to determine the energy of the incident ion beam [27]. The ions enter the detector through a thin Mylar film where they encounter the gas and produce electron-ion pairs. In the presence of the electric field the electrons and ions separate and induce voltage signals on the cathode and anode inside the detector. The anode is subdivided into segments which determine the energy deposited over a corresponding section of the ion path, while the cathode provides a signal proportional to the total ion energy (see Fig. 2). While the total energy measurement is made by the cathode, segmenting of the anode makes it possible to determine the amount of energy deposited on each plate. This in turn allows the detector to discriminate among particles whose energy is the same but which possess different nuclear charges Z. While the detector itself is capable of resolving beams with different E and Z, the energy loss of the beam in the Mylar window at the entrance to the detector limits the maximum attainable M_X for a given charge state q.

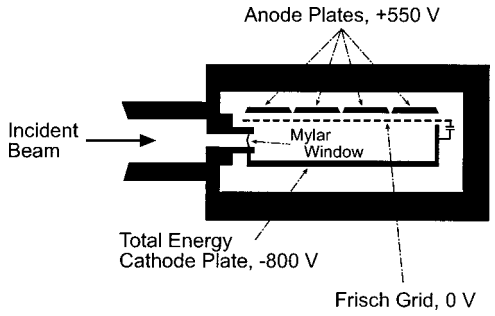

FIG. 2. Schematic cross section of the PRIME Lab gas ionization detector. Notice the Mylar window at the entrance to the detector which prevents the propane gas from entering the beam pipe.

C. Experimental procedure

The samples were placed in copper cathodes attached to an eight-position copper wheel which allowed each sample to be rotated into the path of the Cs^+ beam. The accelerator was tuned to a particular terminal voltage and mass, and after each sample was counted at this voltage for one minute, the injector magnetic field strength was changed to select for the next mass. At the same time the terminal voltage, and the electric fields in both the electrostatic quadrupoles and the electrostatic analyzer were adjusted so that ME/q^2 for the magnets following the accelerator remained constant at their maximum field strengths. It follows that for a fixed charge state q, scanning to higher masses M necessitated working at a lower beam energy E which, however, had to exceed the window cutoff energy. The window cutoff energy is the minimum beam energy required to penetrate the 2.5 μm Mylar window, and is primarily a function of the nuclear charges of both the Mylar and the massive particle.

Since ME/q^2 is held constant during the scan, it was necessary to change to higher charge states in order to detect higher masses. To achieve this we introduced the variational charge state method (VCSM): As the selected mass increased, the beam energy was reduced until it fell below the window cutoff energy, after which the next higher charge state was selected to allow for a higher beam energy. It should be noted that the energy is a function of the charge state (q) and terminal voltage (V_T), along with the voltage (V_p) of the pre-acceleration stage in which atoms from the sample are extracted by the ion source. Hence,

$$E=[(1+q)V_T+V_p]|e|, \tag{4}$$

where $|e|$ is the unit of electric charge. The VCSM allowed us to run at lower charge states which yielded higher transmission efficiencies, and as a result optimized the limits on X/Au for a given M_X.

III. SAMPLES

We present in this section a detailed description of each of the analyzed samples. This information is important in constraining various theoretical models [26], since the limits that follow from our experimental results depend on the known (or presumed) exposures of our samples to cosmic rays or other sources. In all cases, we attempted to obtain samples with the largest possible exposure times to sources which might contain putative SIMPs.

A. Geological samples

To maximize exposure to possible galactic dark matter SIMPs and to any cosmic ray SIMP component, we restricted our geological samples to those residing within ≈ 15 cm of the surface in areas which were relatively inactive geologically. It should be emphasized that gold obtained from near the surface of the Earth may be the result of relatively recent ongoing geological activity such as erosion or deposition. Since bedrock is being continually buried and exhumed, it is generally difficult to determine the length of time during which a given sample was exposed to cosmic rays. However, duration of exposure can be estimated using erosion rates.

Since the actual penetration depth of SIMPs is heavily model dependent, we present three distinct ages for each gold nugget. First, we estimate the time the sample spent in the top meter of the surface, which we calculate from simple estimates involving erosion rates for the region of interest. Since erosion rates vary significantly over the surface of the Earth, we have used a simple model to estimate near surface residency time [7]. This model has been widely used to provide mean minimum estimates of surface residency times [28,29]. Since gold is relatively unreactive and more dense than Earth, it resists removal and generally becomes concentrated in the soil or stream sediment as a residuum. As a result, the above model provides a conservative estimate of the near surface residency time of the sample. Second, we introduce the time since the quartz veins or other mineral deposits containing the gold were formed. Finally, we estimate the age of nucleosynthesis as an upper bound on the age of an Au sample, since it represents the age at which the first heavy elements were formed. We emphasize, however, that any uncertainty in dating the samples only affects the implications to be drawn from our experimental results, and not the results themselves.

1. Western Australia

Our oldest near surface samples come from two different areas in the Leanora District of western Australia: Laverton (28° 37.5′ S, 122° 24.0′ E); and Nullagine (28° 53.2′ S, 122° 19.8′ E). The nuggets were found in the upper few centimeters of soil with a metal detector. This region of Australia is tectonically inactive and, because of its arid climate and low topographic relief, samples from western Australia have some of the longest near-surface exposures of any gold on Earth (1.25 My). The age of mineralization of these samples has been estimated at 2.65×10^9 years (2.65 Gy) [30] (see Table I). For more details on the samples see Table II.

2. Arizona

We have also obtained a sample from the Mineral Park District (Gold Basin) of northwestern Arizona (35° 47.2′ N, 114° 10.7′ W). The sample was found in the upper few

TABLE I. Estimated ages for the geological gold nuggets. Two different ages are presented since the actual penetration depth of SIMPs is model-dependent. For models in which a SIMP stops in the soil layer of material near the surface, the surface age would apply. In contrast, models for which the SIMP penetration depth is much larger suggest the use of the age of mineralization or even the time of Au formation from nucleosynthesis.

Region	Type	Assumed erosion rate	Age
Australia	Surface (within top meter)	0.8 m/My [31,32]	1.25 My
	Mineralization		2.65 Gy [30]
Arizona	Surface	2.5–58 m/My [33]	0.02–0.4 My
	Mineralization		50–70 My [34]
North Carolina	Surface	6–10 m/My [35,36]	0.1–0.2 My
	Mineralization		570 My [37–39]

centimeters of the soil, and includes vein quartz indicating that it was not transported. The sample's discovery location was in the transition region from the tectonically active Basin and Range to the relatively inactive Colorado Plateau. This region of the southwest United States is considered a semi-active tectonic region, with an age of mineralization estimated at 50–70 My [34]. The climate in this region is arid with approximately 20 cm of annual precipitation. The wide range in estimated exposure times presented in Table I reflects the contrasting relief of the region. Areas with deep valleys or canyons tend to have faster erosion rates than plateaus and hilltops. Since our nugget was discovered on a gently-sloping hilltop the lower end of this range is likely most applicable.

As with all North American samples, the Arizona sample is likely to have a much shorter near-surface residency time when compared to the Australian samples. However, this is probably the best that can be expected from North America, and reflects both the recent tectonic activity and faster rates of erosion.

We note in passing that the Arizona nugget had a tarnished appearance, which indicated the presence of contaminants. This was later confirmed by the observation of a large number of contaminating peaks in the total energy spectra. All native gold is an alloy of gold, silver and copper. While the gold is relatively unreactive, the silver and copper will tarnish. If the nugget is in a near-surface oxidizing environment (stream sediment or soil residuum) the silver and copper leach out of the gold over time. This suggests that in contrast to the Australia and North Carolina samples, the Arizona gold nugget has not had as long a residual history. However, one must be cautious and note that the Australia and North Carolina samples generally have lower initial silver contents.

TABLE II. Masses of the geological samples by run. Runs Au2 and Au4 were carried out in charge states $q=+7$ and $q=+9$, respectively, whereas run Au5 used the variational charge state method. As we discuss in the text, different charge states correspond to different mass ranges for M_X. In two instances (Nullagine and Gold Basin) the samples were not entirely consumed following run Au4, and were reused in run Au5.

Region	Sample	Run	Mass [g]
Australia	Laverton	Au2	0.1083 ± 0.0001
		Au4	0.1106 ± 0.0001
		Au5	0.0884 ± 0.0001
	Nullagine	Au4	0.1890 ± 0.0001
		Au5	Same Cathode
Arizona	Gold Basin	Au4	0.3767 ± 0.0001
		Au5	Same Cathode
North Carolina	Golden Valley	Au4	0.3811 ± 0.0001
		Au5	0.1951 ± 0.0001
	Black Run Creek	Au4	0.3774 ± 0.0001

3. North Carolina

Two samples were collected from streams in western North Carolina. These were recovered during placer mining from Golden Valley/McDowell City, and Black Run Creek, all of which were extracted from an area centered on 35° 47′ N, 82° 20′ W. The sample grain sizes range from sub-millimeter to approximately one centimeter and were recovered within the active or recent stream channels that drain disseminated gold deposits formed ~570 million years ago [37–39]. The regional topography has moderate relief, with a climate which receives approximately 100 centimeters of precipitation annually. Rates of erosion are relatively slow in the Appalachian foothills since they are tectonically quiet, and were south of the area affected by glaciation during the Ice Age. Further details on the geology of the region from which these samples were obtained can be found in Ref. [7].

B. Exotic samples

In addition to the previously discussed geological samples, we obtained three ''exotic'' samples: one was gold from the NASA Long Duration Exposure Facility (LDEF) satellite, and a second was gold from the Alternating Gradient Synchrotron (AGS) at Brookhaven National Laboratory. The third sample was a piece of iron meteorite from the Canyon Diablo, Arizona crater. Since these samples came from environments which were very different from those of the geological samples, they expand the discovery opportunity for SIMPs. In addition the histories of these samples were better documented than those for the geological samples.

TABLE III. Masses of the LDEF samples by run. The run mass refers to the amount of Au actually used in the experiment.

Quantity	Value
Diameter	1.585 cm
Thickness	0.5 mm
Run Au4 mass	0.2770 ± 0.0001 g
Run Au5 mass	0.2322 ± 0.0001 g

1. Long Duration Exposure Facility (NASA)

LDEF was in Earth orbit for 69 months from 1984 to 1990, and was designed to provide long-term data on the space environment and its effects on space systems and operations. LDEF was placed into a nearly circular orbit at an altitude of 275 nautical miles (≈ 500 km) and at an inclination of 28.4 degrees. Since LDEF was deployed during a solar minimum and retrieved at a solar maximum, it experienced one-half a solar cycle during its 32 422 Earth orbits.

Our samples were obtained from the Meteoroid and Exposure Module (MEM) which studied the reaction of gold foils to micrometeorite impacts. NASA provided us with 3.9546 ± 0.0002 grams of gold from this experiment, and detailed descriptions of these samples are given in Table III. The MEM experiment tray housed 0.5 mm thick gold foils with a combined cross-sectional area of 1.27 m$\times$1.27 m. (For more details regarding the origin of these samples and the original LDEF experiment, including the sample locations, see Hörz *et al.* [40] and Ref. [7].)

2. Alternating Gradient Synchrotron Beam Dump (BNL)

We were provided with 30.7171 ± 0.0001 grams of Au from the beam dump of an experiment which investigated rare processes in heavy ion collisions with the Alternating Gradient Synchrotron (AGS) at Brookhaven National Laboratory. In experiment E878 [41,42], 3.55×10^{12} gold atoms were incident on an Au strip target which had a thickness of 0.616 cm, corresponding to a 30% interaction length. The thickness of the Au target was chosen so that 22.5% of the incident Au beam interacted, assuming a 6850 mb total inelastic Au+Au cross section [43]. Using this model 3.55×10^{12} gold atoms represents 7.81×10^{11} inelastic Au+Au interactions. The flux of incident Au ions was deposited predominantly in the center centimeter of the target, with a negligible amount deposited near the edges [44].

3. Canyon Diablo Meteorite

We also obtained a 2995.6 gram sample of meteorite which is predominantly iron (92%) and is a fragment of the much larger meteoroid that impacted the Earth $\sim 50\,000$ years ago at Canyon Diablo, Arizona (35° 3′ N, 111° 2′ W). The meteoroid is estimated to have spent ~ 540 million years in interstellar space [45]. Its original mass is estimated to have been $\approx 6 \times 10^7$ kg, and if it were traveling at its estimated speed of 14.5 km/s this would imply that the initial diameter of the meteoroid was greater than 30 m [46].

IV. DISCUSSION AND RESULTS

We present in this section the detailed experimental results obtained from the various samples described above. The object of this experiment was to measure the ratio X/Au, where X denotes the number of hypothetical ${}_{79}X$ anomalous nuclei (having a mass M_X) and Au denotes the number of ${}_{79}\mathrm{Au}$ nuclei in the sample. This ratio is experimentally de-

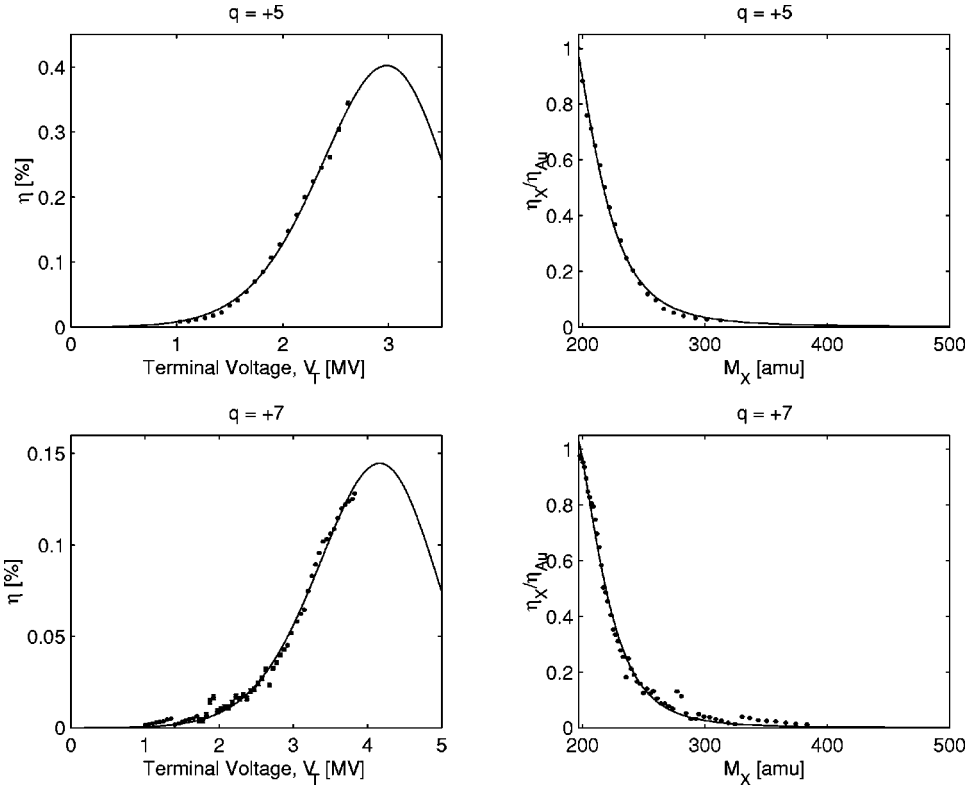

FIG. 3. Stripper efficiency data for charge states $q=+5$ and $q=+7$. For each charge state the figure on the left presents the measured efficiency as a function of terminal voltage, while the corresponding figure on the right presents the same data transformed into a dependence on M_X. Notice that the scales are not the same for $q=+5$ and $q=+7$ since the amplitude of the curves decreases and the peak location shifts with increasing charge state. This behavior is better visualized in Fig. 4 below. For further details see text and Ref. [7].

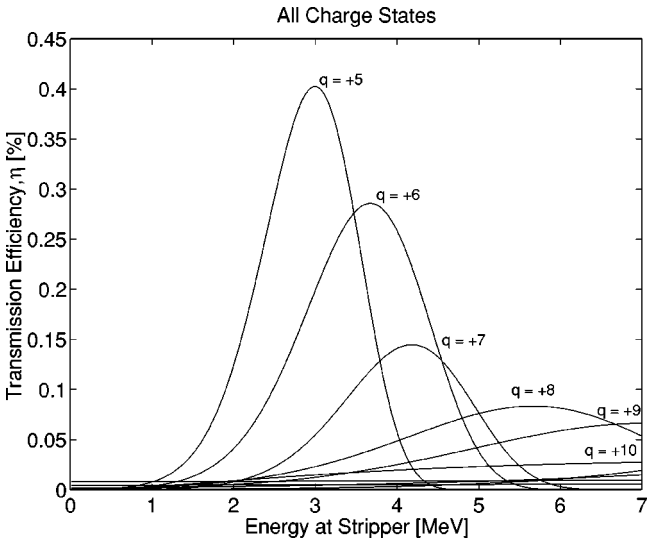

FIG. 4. Stripper efficiency as a function of energy for charge states $q=+5$ to $q=+14$. For charge states $q=+11$ and higher the labels are not included on the plot.

termined by comparing the counting rate, R, of the $_{79}X$ nuclei measured by the detector (in counts per minute, cpm) to the $_{79}$Au beam current, I_{det}, measured by the detector Faraday cup (in nA),

$$\frac{X}{Au}=\frac{R}{I_{det}}\left(\frac{\eta_{Au}}{\eta_X}\right). \tag{5}$$

In Eq. (5) above η_{Au} (η_X) is the transmission efficiency for detecting $_{79}$Au ($_{79}X$). This ratio is included since the transmission efficiency for detecting the heavy isotope is a function of the isotope mass. We must also introduce a factor which converts from cpm to nA so that R is expressed in the same units as I_{det},

$$\begin{aligned}\text{cpm}=&\frac{\text{count}}{\text{min}}\left(\frac{q|e|}{1\ \text{count}}\right)\left(\frac{1.602\times10^{-19}\ \text{C}}{|e|}\right)\\&\times\left(\frac{1\times10^{9}\ \text{nA}}{1\ \text{C/s}}\right)\left(\frac{1\ \text{min}}{60\ \text{s}}\right)\\=&q(2.672\times10^{-12})\ \text{nA},\end{aligned} \tag{6}$$

where $q|e|$ is the common charge of the $_{79}$Au and $_{79}X$ nuclei (in charge state q) selected by the accelerator (see discussion below). Including this factor leads to

$$\frac{X}{Au}=(2.672\times10^{-12})\frac{qR}{I_{det}}\left(\frac{\eta_{Au}}{\eta_X}\right). \tag{7}$$

Since we anticipate a null result we interpret the limits using standard Poisson statistics [47]. In such cases R is replaced by $(-\ln\varepsilon_X)$ where $\varepsilon_X=(1-\text{C.L.})$ and C.L. is the desired confidence limit. The results quoted here are at the 95% C.L. which corresponds to $(-\ln\varepsilon_X)=3.00$.

TABLE IV. X mass, M_X, as a function of charge state, q. The most stringent limits on X/Au for the indicated ranges of M_X were obtained from a beam with the corresponding charge state, q. The application of these constraints comprised the variational charge state method.

Charge state, q	Mass range, M_X [amu]
+5	$200\leqslant M_X<223$
+6	$223\leqslant M_X<324$
+7	$324\leqslant M_X<442$
+8	$442\leqslant M_X<569$
+9	$569\leqslant M_X<723$
+10	$723\leqslant M_X<910$
+11	$910\leqslant M_X<1075$
+12	$1075\leqslant M_X<1302$
+13	$1302\leqslant M_X<1495$
+14	$1495\leqslant M_X<1776$

A. Transmission efficiencies

In order to extract X/Au from the measured $_{79}X$ counting rate and the $_{79}$Au beam current, it is necessary to determine the respective efficiencies for detecting X and Au. In general the total beam transmission efficiency for either X or Au is the product of the separate efficiencies for each element of the AMS, such as a pair of collimating slits or the Ar gas stripper. However, each of these efficiencies is approximately the same for X and Au, with the exception of the Ar stipper efficiency which depends on ion velocity and thus on M_X. Hence for practical purposes η_{Au}/η_X is essentially the ratio of the respective efficiencies in the Ar stripper. The SIMP efficiencies at different masses can be modeled by those of an Au beam with the same velocity, since electron stripping in Ar at the terminal is a function of ion velocity and nuclear charge (Z) only. An example of the results from this procedure is provided in Fig. 3 which presents our data for charge states $q=+5$ and $q=+7$ as a function of the terminal voltage. In effect we are evaluating the efficiency of stripping $Z=197$ to the desired charge state as a function of ion velocity. Since the ion velocity is a function of the $_{197}X$ mass

TABLE V. Summary of guide beams. For each of the guide beams in the first column we list the terminal voltage V_T, in MV, at which the corresponding guide beam makes it through the magnetic and electrostatic components. We also list the final beam energy in MeV, and the beam width ΔV_T at that terminal voltage. See text and Ref. [7] for further discussion.

Guide beam	V_T [MV]	Energy [MeV]	ΔV_T [MV]
Au^{+12}	6.945 ± 0.003	90.30 ± 0.05	0.155 ± 0.003
Au^{+9}	5.070 ± 0.003	50.71 ± 0.05	0.095 ± 0.003
Au^{+5}	2.613 ± 0.003	15.69 ± 0.05	0.052 ± 0.003
Au^{+4}	1.995 ± 0.003	9.99 ± 0.05	0.04 ± 0.003
Au^{+3}	1.397 ± 0.003	5.60 ± 0.05	0.03 ± 0.003
Cu^{+1}	0.972 ± 0.003	1.96 ± 0.05	0.025 ± 0.003
Au^{+2}	0.828 ± 0.003	2.50 ± 0.05	0.025 ± 0.003

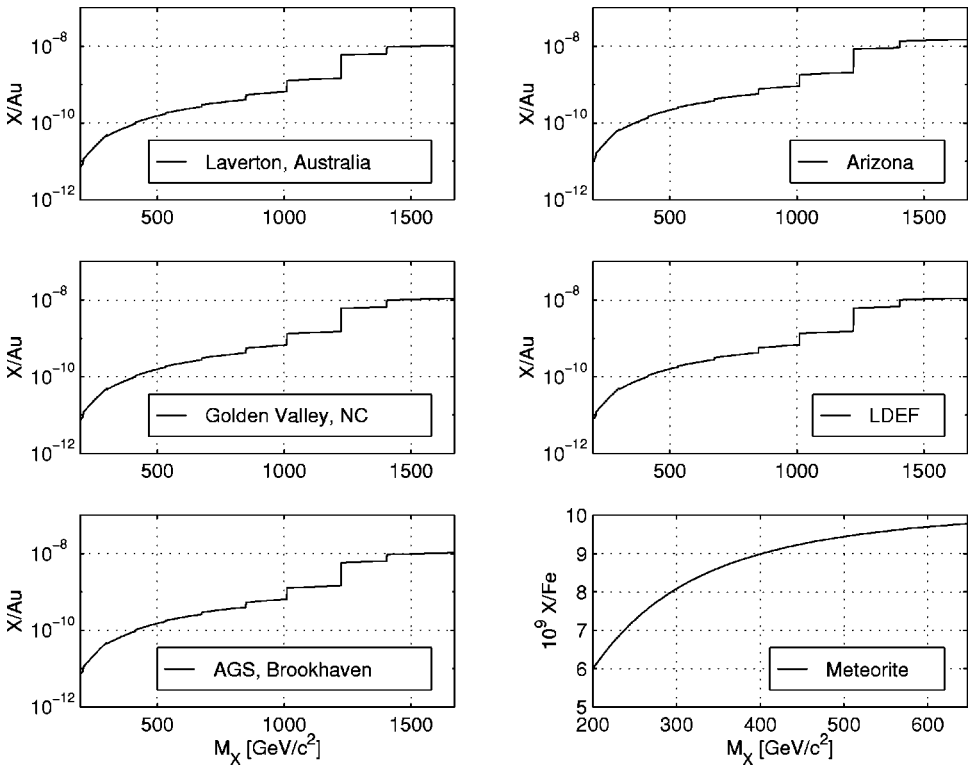

FIG. 5. The X/Au ratios for the 5 different $_{79}$Au samples, along with the X/Fe ratio for the $_{26}$Fe meteorite. Since no evidence for anomalous nuclei was seen in any of the samples, the limits expressed are the bounds on the corresponding ratios at the 95% confidence level. See text and Ref. [7] for further details.

we have transformed the raw data (which are given in the left hand plots) to the quantities relevant in our search, namely M_X and the ratio of the efficiencies. The plots on the right are in terms of these transformed quantities which start at $M_X = M_{Au}$. The uncertainties for the higher charge states were slightly larger than for the lower charge states since fewer data points were taken, but the trend remained the same for all q (see Fig. 4).

This technique of modeling the X efficiency with Au must then be separately applied to each selected charge state denoted by q. As we have discussed above, q varies throughout the experiment, being chosen appropriately to maximize the efficiency for a given range of M_X [7] (see Table IV). As a result it was necessary to determine the transmission efficiency as a function of SIMP mass for each charge state. As the charge state increases the stripper yield decreases as evidenced in Fig. 4.

B. Other experimental considerations

As noted previously, we relied on the presence of various guide beams to check the tune of the AMS throughout the scan up to 1.67 TeV/c^2. In addition the guide beams were useful in calibrating the gas ionization detector while simultaneously determining the minimum beam energy necessary to penetrate the Mylar entrance window into the detector. Finally the guide beams were used to determine the voltage step size as a function of the terminal voltage, which helped

TABLE VI. Final experimental bounds on X/Au and X/Fe from the various samples reported at the 95% C.L. For most of the samples the variational charge state method (VCSM) described in the text was employed to reach the highest possible mass, which was 1.67 TeV/c^2. To save time in the scans, the Nullagine, Black Creek, and meteorite samples were only run at $q=+9$, which limits the maximum M_X to 0.65 TeV/c^2.

Sample	Run	Mass range [GeV/c^2]	X/Au Limit range
AGS	Au5	188–1669	$6.2\times10^{-12}-1.0\times10^{-8}$
LDEF	Au5	188–1669	$6.6\times10^{-12}-1.1\times10^{-8}$
Laverton	Au5	188–1669	$6.3\times10^{-12}-1.1\times10^{-8}$
Nullagine	Au4	188–647	$7.5\times10^{-11}-2.7\times10^{-9}$
Arizona	Au5	188–1669	$8.9\times10^{-12}-1.5\times10^{-8}$
Golden Valley, NC	Au5	188–1669	$6.5\times10^{-12}-1.1\times10^{-8}$
Black Run Creek, NC	Au4	188–647	$6.6\times10^{-11}-2.4\times10^{-9}$
Sample	Run	Mass range [GeV/c^2]	X/Fe Limit range
Meteorite	Au4	188–647	$5.6\times10^{-9}-9.7\times10^{-9}$

optimize run times. The guide beams we used are given in Table V which presents their terminal voltages, energies and beam widths.

The detector calibration, and the calculation of the window cutoff energy, were performed in the same study using the Au^{+9} guide beam. To perform this test the Au peak in the detector total energy spectrum was monitored, while the total energy of the guide beam was slowly decreased. This allowed us to precisely calibrate the detector behavior as a function of beam energy for $Z=79$. Once the beam energy reached the window cutoff energy, a sudden drop in the detector counting rate was observed which corresponded to a beam energy of 13.7 ± 0.2 MeV for a 2.5 μm thick Mylar film. It should be noted that, once calibrated, the gas ionization detector resolves beams with different energies and different nuclear charges, *Z*. Thus, we provide stringent limits even in the presence of a small $_{204}$Tl or $_{209}$Bi contamination. For more information regarding this procedure and the detector see Refs. [7] and [27].

C. Experimental results

Our results are presented in Fig. 5 and Table VI. Figure 5 presents the ratios X/Au for five different gold samples that were run up to 1.67 TeV/c^2 along with the X/Fe for the iron meteorite sample. Each figure presents the limit on X/Au as a function of the X mass M_X, in GeV/c^2. Note that for each sample two trends are important: First the limits become less stringent as M_X increases. This is a consequence of the fact that higher M_X corresponds to a lower beam velocity given that ME/q^2 is fixed. Since a greater difference between the beam velocity and the Bohr velocity results in a lower stripper yield, stripping becomes less efficient with increasing M_X (see Fig. 3). Secondly we note the presence of discontinuous steps which reflect the change from one observed charge state to another. As discussed previously, changing from one charge state to another using the VCSM optimizes X/Au while simultaneously keeping the beam energy above the window cutoff energy. Although this procedure results in a less stringent limit, it permits a scan to higher masses.

Given the proximity of the Laverton and Nullagine regions we assumed that exposure in one also took place in the other, and hence only the Laverton sample was run using the VCSM. The same assumption was also applied to the North Carolina samples, and this allowed us to minimize the total run time for the high mass scan using the VCSM to selected samples. The X/Au ratios for the five gold samples along with the X/Fe ratio for the meteorite are shown in Fig. 5. No evidence for anomalous nuclei X was found in any of the gold samples or in the iron meteorite, and hence the limits shown in Fig. 5 and Table VI are the bounds on X/Au and X/Fe at the 95% confidence level (C.L.). We see from the table that for anomalous nuclei with masses ≈ 1.7 TeV/c^2 the bounds are on the order 1×10^{-8}.

V. CONCLUSIONS

We have presented in this paper new experimental limits on the abundances of anomalously heavy isotopes $_ZX$ with $Z=26$ and $Z=79$. Since our primary focus has been on detecting SIMPs, we have devoted considerable effort to obtaining samples with exposure times to sources (and hence SIMPs) which are both long and reasonably well-known. This is evidently true for the LDEF sample, and even more so for the AGS sample, where the incident flux of gold atoms was well-known. For the geological samples, we have been able to infer a range of exposure times on the basis of estimated erosion rates.

Although our primary focus has been to report these limits as constraints on the mass M_X of a hypothetical massive SIMP, our results can also be interpreted as setting limits on anomalous stable heavy Au and Fe nuclei containing a large neutron excess. It should be emphasized that although the limits themselves are model independent, the implications to be drawn from them are not, and require additional theoretical assumptions. We show in Ref. [26] how these results exclude various regions of the $\sigma_{SN}-M_S$ plane where σ_{SN} is the SIMP-nucleon cross section and M_S is the SIMP mass. Specifically the implications of our results for the SIMP contribution to the cosmological density parameter are discussed in detail [26].

Our results complement those obtained by previous groups. Hemmick *et al.* [3] carried out a similar SIMP search in light nuclei. For their heaviest nucleus, fluorine, they found $X/F<10^{-11}-10^{-16}$. As previously mentioned, the present paper extends this technique to heavier nuclei where SIMPs may bind preferentially [7,8,26], although this comes at the cost of reduced sensitivity. Rich *et al.* [5] and Bernabei *et al.* [6] have set limits on massive SIMPs from scattering experiments, where exposure times are considerably shorter, but the detection efficiencies are better known. Comparing our results to those obtained from scattering experiments is not straightforward, since this requires knowledge of SIMP properties such as interaction cross sections and is beyond the scope of the present paper. (For one such application of these results see Ref. [26].) Thus, while each experiment provides new information on SIMPs, relating different experiments to one another requires a more detailed SIMP model, such as those considered in Refs. [13,25,26].

ACKNOWLEDGMENTS

The authors are deeply indebted to Sam Aronson and Mike Bennett for providing us with the AGS sample, and for several helpful communications. We are also deeply indebted to Friedrich Hörz and NASA for providing the LDEF sample, and for discussions regarding its history. E.F. wishes to acknowledge and thank the late Idella Marx for making the meteorite sample available to us. We also wish to thank David E. Miller, Glenn Sembroski, Pankaj Sharma, and the staff of PRIME Lab for their help on the experiment. V.T. wishes to thank E.T. Herrin for helpful discussions. This work was supported in part by the U.S. Department of Energy under Contract No. DE-AC02-76ER01428, and National Science Foundation Grant No. 9809983-EAR.

[1] D. Javorsek II, D. Elmore, E. Fischbach, T. Miller, D. Oliver, and V. Teplitz, Phys. Rev. D **64**, 012005 (2001).
[2] D. Javorsek II, D. Elmore, E. Fischbach, D. Granger, T. Miller, D. Oliver, and V. Teplitz, Phys. Rev. Lett. **87**, 231804 (2001).
[3] T.K. Hemmick *et al.*, Phys. Rev. D **41**, 2074 (1990).
[4] E.B. Norman, S.B. Gazes, and D.A. Bennett, Phys. Rev. Lett. **58**, 1403 (1987).
[5] J. Rich, R. Roccia, and M. Spiro, Phys. Lett. B **194**, 173 (1987).
[6] R. Bernabei *et al.*, Phys. Rev. Lett. **83**, 4918 (1999).
[7] D. Javorsek II, Ph.D. thesis, Purdue University, 2001.
[8] R.N. Mohapatra, F. Olness, R. Stroynowski, and V.L. Teplitz, Phys. Rev. D **60**, 115013 (1999).
[9] R.N. Mohapatra and V.L. Teplitz, Phys. Rev. Lett. **81**, 3079 (1998).
[10] S. Dimopoulos, D. Eichler, R. Esmailzadeh, and G.D. Starkman, Phys. Rev. D **41**, 2388 (1990).
[11] E. Nardi and E. Roulet, Phys. Lett. B **245**, 105 (1990).
[12] R.S. Chivukula, A.G. Cohen, S. Dimopoulos, and T.P. Walker, Phys. Rev. Lett. **65**, 957 (1990).
[13] G.D. Starkman, A. Gould, R. Esmailzadeh, and S. Dimopoulos, Phys. Rev. D **41**, 3594 (1990).
[14] V.S. Berezinskiĭ and B.L. Ioffe, Sov. Phys. JETP **63**, 920 (1986).
[15] D.J.H. Chung, G.R. Farrar, and E.W. Kolb, Phys. Rev. D **57**, 4606 (1998).
[16] I.F.M. Albuquerque, G.R. Farrar, and E.W. Kolb, Phys. Rev. D **59**, 015021 (1998).
[17] R.N. Mohapatra and S. Nussinov, Phys. Rev. D **57**, 1940 (1998).
[18] R.N. Mohapatra and S. Nandi, Phys. Rev. Lett. **79**, 181 (1997).
[19] S. Raby, Phys. Rev. D **56**, 2852 (1997).
[20] Z. Chacko, B. Dutta, R.N. Mohapatra, and S. Nandi, Phys. Rev. D **56**, 5466 (1997).
[21] V. Berezinsky and M. Kachelrieß, Phys. Lett. B **422**, 163 (1998).
[22] A. Mafi and S. Raby, Phys. Rev. D **62**, 035003 (2000).
[23] A. Mafi and S. Raby, Phys. Rev. D **63**, 055010 (2001).
[24] D.N. Spergel and P.J. Steinhardt, Phys. Rev. Lett. **84**, 3760 (2000).
[25] B.D. Wandelt *et al.*, astro-ph/0006344 (2000).
[26] D. Javorsek II, E. Fischbach, and V. Teplitz, Astrophys. J. **568**, 1 (2002).
[27] D. L Knies and D. Elmore, Nucl. Instrum. Methods Phys. Res. B **92**, 134 (1994).
[28] D. Granger, J. Kirchner, and R. Finkel, J. Geol. **104**, 249 (1996).
[29] D. Granger, D. Fabel, and A. Palmer, Geol. Soc. Am. Bull. **113**, 825 (2001).
[30] D. Groves, M. Barley, and S. Ho, Economic Geology Monograph **6**, 71 (1989).
[31] P. Bierman and J. Turner, Quat. Res. **44**, 378 (1995).
[32] R. Garrels and F. McKenzie, *Evolution of Sedimentary Rocks* (Norton, New York, 1971).
[33] S. Schumm, U.S. Geol. Surv. Prof. Paper **454-H**, (1963).
[34] S. Titley, Economic Geology Monograph **6**, 626 (1989).
[35] M. Pavich, L. Brown, J. Valette-Silver, J. Kein, and R. Middleton, Geology **13**, 39 (1985).
[36] J. Dymond and M. Lyle, in *Material Fluxes on the Surface of the Earth* (National Academy Press, Washington, DC, 1994), p. 125.
[37] J. Reid (private communication).
[38] J. Gair and J. D'Agostino, U.S. Geol. Surv. Prof. Paper **I-1251-H** (1986).
[39] J. Gair, U.S. Geol. Surv. Prof. Paper **1462** (1989).
[40] F. Hörz, R. Bernhard, J. Warren, T. See, D. Brownlee, M. Laurance, S. Messenger, and R. Peterson, *LDEF—69 Months in Space: First LDEF Post-Retrieval Symposium*, NASA Conference Publication No. 3134 (NABA, Greenbelt, MD, 1991), p. 487.
[41] M.J. Bennett *et al.*, Phys. Rev. C **58**, 1155 (1998).
[42] D. Beavis *et al.*, Phys. Rev. Lett. **75**, 3078 (1995).
[43] M.J. Bennett (private communication).
[44] S. Aronson (private communication).
[45] D. Heymann, M. Lipshutz, B. Nielson, and E. Anders, J. Geophys. Res. **71**, 619 (1966).
[46] M. Lipshutz (private communication).
[47] Particle Data Group, R.M. Barnett *et al.*, Phys. Rev. D **54**, 1 (1996).